

A Monte Carlo Tree Search Framework for Quantum Circuit Transformation

Xiangzhen Zhou, Yuan Feng, Sanjiang Li

Abstract—In Noisy Intermediate-Scale Quantum (NISQ) era, quantum processing units (QPUs) suffer from, among others, highly limited connectivity between physical qubits. To make a quantum circuit executable, a circuit transformation process is necessary to transform it into a functionally equivalent one so that the connectivity constraints imposed by the QPU are satisfied. While several algorithms have been proposed for this goal, the overhead costs are often very high, which degenerates the fidelity of the obtained circuits sharply. One major reason for this lies in that, due to the high branching factor and vast search space, almost all these algorithms only search very *shallowly* and thus, very often, only (at most) locally optimal solutions can be reached. In this paper, we propose a Monte Carlo Tree Search (MCTS) framework to tackle the circuit transformation problem, which enables the search process to go much deeper. The general framework supports implementations aiming to reduce either the size or depth of the output circuit through introducing SWAP or remote CNOT gates. The algorithms, called MCTS-Size and MCTS-Depth, are polynomial in all relevant parameters. Empirical results on extensive realistic circuits and IBM Q20 Tokyo show that the MCTS-based algorithms can reduce the size (depth, resp.) overhead by, in average, 66% (84%, resp.) when compared with $t|ket\rangle$, an industrial level compiler.

Index Terms—NISQ, quantum circuit transformation, qubit mapping, Monte Carlo tree search, heuristic search.

I. INTRODUCTION

With Google’s recent conspicuous, though arguable, success in demonstrating quantum supremacy in a 53-qubit quantum processor [1], NISQ (Noisy Intermediate-Scale Quantum) devices have attracted rapidly increasing interests from researchers in both academic and industrial communities. *Quantum processing units* (QPUs) in the NISQ era only support a limited set of basic operations (elementary quantum gates) and often suffer from high gate errors, short coherence time, and limited connectivity between physical qubits. In order to run a quantum algorithm, described as a quantum circuit, we need to *compile* the circuit (referred to as *logical circuit* henceforth) into a functionally equivalent *physical circuit* executable on the QPU. The compilation includes two basic processes. In the *decomposition* process, gates in the logical circuit are decomposed, or transformed, into elementary gates supported by the QPU [2], [11]. The *transformation* process, known as *quantum circuit transformation* (QCT) [6], [34] or *qubit mapping* [15], [16], [32], is then performed on

the generated circuit, which further consists of two steps: *initial mapping* and *qubit routing*. The former maps qubits in a logical circuit, called *logical qubits*, to the ones in the QPU, called *physical qubits*; while the latter transforms a circuit through adding ancillary operations like SWAP gates to ‘route’ physical qubits in order to make all multi-qubits gates executable.

Both the decomposition and the transformation processes have been studied extensively in the literature. As there are now standard decomposition processes (see [20], [24]), in this paper, we focus on the transformation one, and assume that gates in the input logical circuit have been well decomposed into elementary gates that are supported by the QPU. Furthermore, we assume that an initial mapping is given, which can be obtained by employing, say, the greedy strategy [35], [22], [7], the reverse traversal technique [15], the simulated annealing based algorithm [34], or the subgraph isomorphism based methods [16].

To reduce the gate overheads in the qubit routing step, many algorithms have been proposed aiming at minimising gate counts [35], [34], [16], [17], circuit depths [14], [32], [3], [31] or circuit error [21], [18]. These algorithms can be roughly classified into two broad categories. The first category consists of algorithms that try to reformulate QCT as a planning or optimisation problem and solve it by applying off-the-shelf tools [3], [31], [28], [23], [30], [18], [8]. However, as shown in [28], [6], QCT is NP-complete in general. Algorithms in this category are usually highly unscalable when the size of input circuits becomes large.

In contrast, algorithms in the second category use heuristic search to construct the output quantum circuit step by step from the original input quantum circuit [15], [22], [35], [28], [10], [34]. Experimental results show that customised heuristic search algorithms are more promising in transforming large-scale circuits, but usually there is still a considerable gap between the output circuit and an optimal one. The reason partially lies in the limited search depth in most of these algorithms. To achieve efficiency, one either divides the circuits into layers and tries to execute the gates layer-wise [35], or simply considers only the direct effect of a single move (i.e., SWAP) (see e.g., [15], [6], [7]). This leads to a very shallow search depth. The Simulated Annealing and Heuristic Search algorithm (SAHS) [34] and the Filtered and Depth-Limited Search approach (FiDLS) [16] can go one or two steps further, but exploring even more seems impractical as the searching process will become very slow if many qubit connections are present in the QPU.

Inspired by the recent spectacular success of Monte Carlo

Xiangzhen Zhou is with State Key Lab of Millimeter Waves, Southeast University, Nanjing 211189, China and Centre for Quantum Software and Information, University of Technology Sydney, NSW 2007, Australia.

Sanjiang Li and Yuan Feng are with Centre for Quantum Software and Information (QSI), Faculty of Engineering and Information Technology, University of Technology Sydney, NSW 2007, Australia.

E-mail: {sanjiang.li, yuan.feng}@uts.edu.au

Tree Search (MCTS) in Computer Go play [25], [26], in this paper, we propose an MCTS framework for the QCT problem. Although first designed for solving computer games, MCTS has found applications in many domains which can be represented as trees of sequential decisions [4]. MCTS is a flexible statistical anytime algorithm, which can be used with little or no domain knowledge [4]. The basic idea behind MCTS is to explore and exploit, in a balanced way, a search tree in which each node represents a game state and each branch a legal move starting from that state. Given the current game state, the aim is to select the most promising move by exploring a search tree rooted with this state, based on random sampling of the search space. This is achieved through the following five steps: (1) *Selection*. Starting from the root, we first select successively a child node until a leaf node is reached; (2) *Expansion*. Expand the selected leaf node with one or more child nodes each of which corresponding to a legal move; (3) *Simulation*. Play out the task to completion by selecting subsequent moves randomly; (4) *Backpropagation*. Backpropagate the simulation result (winning, losing, or the reward points collected) towards the root node to update the values of nodes along the way; (5) *Selection*. After repeated a sufficient number of times, we then select the best move (with the largest value) and move to the next game state.

Example 1. We show how to conduct a full playout based on a search tree as shown in Fig. 1(a). Suppose a simple strategy only choosing child with maximum winning rate¹ is used in Selection. Then starting from root node 0, nodes 2 and 6 with maximum #wins/#simulations values 4/6 and 2/2 among their peers according to the evaluation table in Fig. 1(c) will be chosen successively. Because node 6 is a leaf, it will be expanded and its child nodes 8 and 9, as shown in the dashed box of Fig. 1(b), will be opened. After Expansion, one or more newly opened nodes will be chosen to perform simulations. In this example, both nodes 8 and 9 are chosen to execute 2 random simulations and the results are assumed to be 0/2 and 1/2 respectively. After all simulations in node 8 are done, the result will be back propagated to root node 0 through nodes 6 and 2, and their values will be updated and are marked red in the ‘EABP1’ column of Fig. 1(c). The same operation applies after the simulations in node 9 are finished and the updated values can be found in the ‘EABP2’ column.

Our MCTS framework for the QCT problem also consists of these five major modules. In the framework, we adopt a fast random strategy for simulation and carefully design a scoring mechanism which takes both short and long-term rewards into consideration. Based on the five modules and the scoring mechanism, an algorithm, abbreviated as MCTS-Size, is proposed to optimise the size of the output circuit. The algorithm is polynomial in all relevant parameters and experiments on an extensive set of realistic benchmark circuits show that the search depth can easily exceed most, if not all, existing algorithms. This deep search method can reduce the gate overhead of the output physical circuits by a large margin

when compared with the state-of-the-art algorithms [34], [16], [7] on IBM Q20.

Although aiming to optimise the circuit size in terms of gate numbers, MCTS-Size also reduces the depth of the output circuit significantly. When compared with $t|ket\rangle$ introduced in [7], a state-of-the-art and industrial level algorithm aiming at depth optimisation, MCTS-Size reduces the circuit size and depth overheads by, respectively, 66% and 75% on IBM Q20 (cf. Table I). More importantly, as our MCTS framework is flexible, it can be easily adapted to accommodate various optimisation criteria. To exemplify this feature, we design MCTS-Depth by introducing two very simple modifications to MCTS-Size. Experimental results on IBM Q20 show that, compared to $t|ket\rangle$ again, MCTS-Depth is able to reduce the depth overhead up to 84%.

This paper is a significant extension of the conference paper [33] presented at ICCAD’20. Among others, we have made the following major extensions: (a) aiming to optimise the output circuit depth, we design the MCTS-Depth algorithm (cf. Sec. IV) (note that [33] only considered optimisation of the output circuit size); (b) to further demonstrate the flexibility of our framework, we incorporate remote CNOT gates into the MCTS-based algorithms (cf. Sec. V); (c) we describe in detail the parameter selection process and empirically compare the search depth of the MCTS-Size algorithm with that of SAHS [34] (cf. Sec. VI); and (d) we present detailed and additional empirical evaluation results (considering depth reduction as well as the effect of remote CNOT gates) on both IBM Q20 and a hypothetical grid-like QPU, called Grid 5×4 , which also has 20 qubits but fewer edge connections than IBM Q20 (cf. Sec. VI).

The remainder of this paper is organised as follows: Sec. II provides some background knowledge about quantum computation and summarises the state-of-the-art of the quantum circuit transformation problem. Sec. III then presents a detailed description of the MCTS framework as well as a theoretical analysis. The adapted depth-optimisation algorithm is presented in Sec. IV. After that, we show how to incorporate remote CNOT in the MCTS-based algorithms in Sec. V. Empirical evaluations of both MCTS-based algorithms on an extensive set of realistic benchmark circuits and on both IBM Q20 and Grid 5×4 are presented in Sec. VI. The last section concludes the paper with an outlook.

II. QUANTUM CIRCUIT TRANSFORMATION

In classical computing, data are stored in the form of bits which have two states, 0 and 1. In contrast, data in quantum computing are stored in *qubits*, which also have two basis states represented by $|0\rangle$ and $|1\rangle$, respectively. However, unlike a classical bit, a qubit can be in the superposition $\alpha|0\rangle + \beta|1\rangle$ of basis states, where α and β are complex numbers satisfying $|\alpha|^2 + |\beta|^2 = 1$.

The state of a qubit can be changed by quantum gates, which are mathematically represented by unitary matrices. Fig. 2 depicts three important quantum gates used in this paper: Hadamard, CNOT and SWAP gates. Hadamard is a single-qubit gate that has the ability to generate superposition: it

¹The strategy for *Selection* in practice is much more complex than this and should take both evaluations and time of visits into account. Interested readers can refer to [13], [5] for further details.

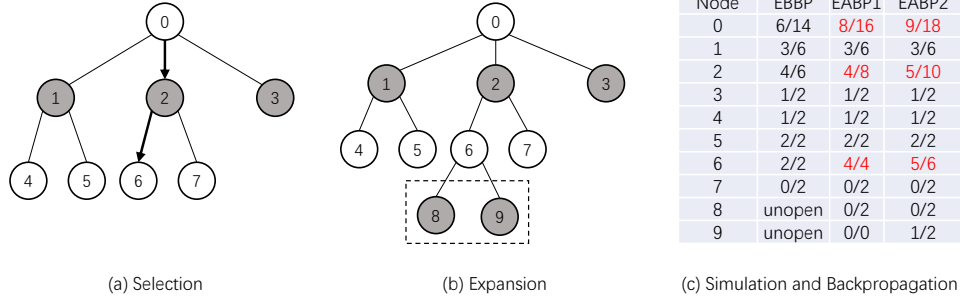


Fig. 1. Example for one playout in MCTS. Each grey or white node in (a) and (b) represents a legal move made by the corresponding player. The last three columns in (c) represent, respectively, evaluations in each node before, after the first, and after the second *Backpropagation*. The evaluation is defined as $\#wins/\#simulations$ obtained by *Simulation* and *Backpropagation*.

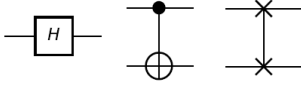


Fig. 2. Hadamard, CNOT and SWAP gates (from left to right).

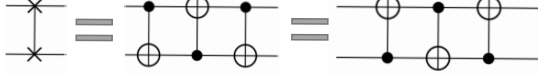


Fig. 3. The decomposition of a SWAP into three CNOT gates.

maps $|0\rangle$ to $(|0\rangle + |1\rangle)/\sqrt{2}$ and $|1\rangle$ to $(|0\rangle - |1\rangle)/\sqrt{2}$. CNOT and SWAP are both two-qubit gates. CNOT flips the target qubit depending on the state of the control qubit; that is, CNOT: $|c\rangle|t\rangle \rightarrow |c\rangle|c \oplus t\rangle$, where $c, t \in \{0, 1\}$ and \oplus denotes exclusive-or. SWAP exchanges the states of its operand qubits: it maps $|a\rangle|b\rangle$ to $|b\rangle|a\rangle$ for all $a, b \in \{0, 1\}$. Note that a SWAP gate can be decomposed into three CNOT gates as shown in Fig. 3.

Quantum gates can be concatenated to form complex *circuits* which, together with measurements, are used to describe quantum algorithms. A circuit is usually denoted by a pair (Q, C) , where Q is a set of qubits and C a sequence of quantum gates on Q . Sometimes we also call C a circuit when Q is clear from the context. Fig. 4 shows a circuit where $Q = \{q_0, \dots, q_4\}$, $C = (g_0, \dots, g_4)$, $g_0 = \text{CNOT}(q_0, q_2)$, $g_1 = \text{CNOT}(q_3, q_4)$, etc. Here each CNOT is annotated with the qubits on which they are applied.

A. Quantum Circuit Transformation

As mentioned in the introduction, to run a quantum circuit on a given QPU in the NISQ era, we need to transform it so that the connectivity constraints imposed by the QPU are all satisfied. Such connectivity constraints are typically described as an undirected and connected graph $AG = (V, E)$, called the *architecture graph* [6], where V denotes the set of physical qubits of the QPU and E the pairs of physical qubits on which a two-qubit gate can be applied.

Note that by a standard process [20], any quantum circuit can be decomposed into a functionally equivalent one which consists of only CNOT and single-qubit gates. Furthermore, as

single-qubit gates can be executed directly on a QPU (connectivity constraints only prevent two-qubit gates from applying on certain pairs of physical qubits), if not otherwise stated, we assume that single-qubit gates have been removed and the circuit to be transformed consists solely of CNOT gates.² Note that this is only a technical assumption and, whenever necessary, we can always add back the corresponding single-qubit gates (cf. Sec. IV).

An important notion related to quantum circuits which plays a key role in QCT is the *dependency graph*. Let $C = (g_0, g_1, \dots)$ be a quantum circuit. We say gate g_i in C *depends* on g_j if $j < i$ and they share at least one common qubit. The dependence is *direct* if there is no gate g_k with $j < k < i$ such that g_i depends on g_k and g_k depends on g_j . In general, we can construct a directed acyclic graph (DAG), called the dependency graph [12], to characterise the dependency between gates in a circuit. Specifically, each node of the dependency graph represents a gate and each directed edge the direct dependency relationship between the gates involved. With the help of dependency graph, any quantum circuit C can be divided into different *layers* such that gates in the same layer can be executed in parallel. The first or front layer, denoted by $\mathcal{L}_0(C)$, consists of the gates which have no parents in the DAG. The second layer, $\mathcal{L}_1(C)$, is then the front layer of the DAG obtained by deleting all gates in $\mathcal{L}_0(C)$. Analogously, we can define the i -th layer of a circuit for any $i \geq 0$.

Example 2. Fig. 4 shows an example of a quantum circuit (left) and its dependency graph (right), from which we can see that the front layer of the circuit consists of g_0 and g_1 , the second g_2 , the third g_3 , and the fourth g_4 .

Another key notion for QCT is a qubit mapping τ which allocates logical qubits Q to physical qubits V so that for any $q_i, q_j \in Q$, $\tau(q_i) = \tau(q_j)$ if and only if $i = j$. Given a logical circuit (Q, C) and an architecture graph AG , a two-qubit gate $g = \text{CNOT}(q_i, q_j)$ in C is called *executable* by τ if $\tau(q_i)$ and $\tau(q_j)$ are adjacent in AG , and g is either in the front layer of C or all the gates it depends on are executable. Note that in general it is impossible that all two-qubit gates in a circuit are executable by a single mapping. Once no gates

²This implies that we cannot simplify the circuits by, say, cancelling out consecutive CNOT gates acting on the same pair of qubits.

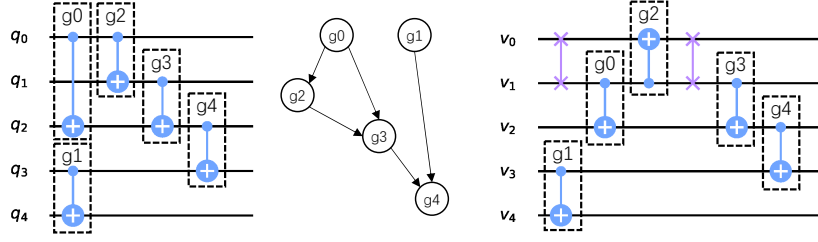


Fig. 4. A quantum circuit (left), its dependency graph (middle) and the circuit after transformation (right).

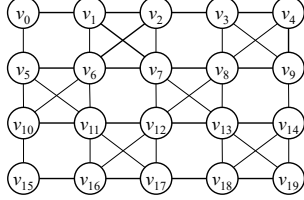


Fig. 5. The architecture graph for IBM Q20.

are executable by the current mapping τ , a QCT algorithm seeks to insert into the circuit some ancillary SWAP gates to change τ into a new one so that more gates are executable. This insertion-execution process is iterated until all gates from the input circuits are executed. To illustrate the basic ideas, we revisit the circuit on the left side of Fig. 4.

Example 3. We transform the logical circuit $LC = (Q, C^l)$ shown in Fig. 4 into a physical one $PC = (V, C^p)$ satisfying the architecture graph AG in Fig. 5. Suppose the initial qubit mapping τ is given as a naive one which maps q_i to v_i , $0 \leq i \leq 4$.

- 1) Since $\tau(q_3) = v_3$, $\tau(q_4) = v_4$, and v_3 and v_4 are adjacent in AG , gate g_1 in C^l is already executable by τ . Thus we initialise PC as a physical circuit with $V = \{v_0, \dots, v_{19}\}$ containing only a single CNOT gate acting on v_3 and v_4 , and delete g_1 from C^l . Thus now, $C^l = (g_0, g_2, g_3, g_4)$ and $C^p = (CNOT(v_3, v_4))$.
- 2) As no gates in C^l is executable by τ , we have to insert a SWAP (or a sequence of them) to get a new mapping which admits more CNOT gates from C^l executable. In this example, we choose to add $SWAP(v_0, v_1)$ to C^p , which in effect converts τ into τ' that maps q_0 to v_1 and q_1 to v_0 . Now g_0 , which acts on q_0 and q_2 , is executable (since v_1 and v_2 are adjacent in AG). Similarly, g_2 is executable as well. Thus they can be deleted from C^l and added into C^p (with the operand qubits changed accordingly). Consequently, now $C^l = (g_3, g_4)$ and

$$C^p = (CNOT(v_3, v_4), SWAP(v_0, v_1), CNOT(v_1, v_2), CNOT(v_1, v_0)).$$

- 3) Proceeding in a similar way, we add another $SWAP(v_0, v_1)$ to C^p to convert τ' back to τ so that g_3 and g_4 are executable. After deleting them from C^l and adding them into C^p , we have $C^l = \emptyset$ and the final

physical circuit becomes

$$C^p = (CNOT(v_3, v_4), SWAP(v_0, v_1), CNOT(v_1, v_2), CNOT(v_1, v_0), SWAP(v_0, v_1), CNOT(v_1, v_2), CNOT(v_2, v_3)),$$

which satisfies all the connectivity constraints of AG . The final physical circuit is shown in Fig. 4 (right).

B. Heuristic Search Algorithms

Recall that given a logical circuit LC_0 , an architecture graph AG , and an initial qubit mapping τ_{ini} , a QCT process aims to output a physical circuit which respects all the connectivity constraints in AG . To present this process as a search problem, we need to first define the notion of states. Naturally, a *state* of the QCT process is a triple $s = (\tau, PC, LC)$, where τ is a qubit mapping describing the current allocation of logical qubits, PC is the physical circuit that consists of all gates that have been executed so far and the auxiliary SWAP gates inserted, and the logical circuit LC consists of the remaining gates to be executed. Sometimes we denote by $LC(s)$ and $PC(s)$ the logical and the physical circuits of s , respectively.

A *legal action* in the QCT process can be either a SWAP operation (corresponding to an edge in AG) or a sequence of SWAP operations.³ Let $s = (\tau, PC, LC)$ be the current state, and suppose an action $SWAP(v_i, v_j)$ is taken on s . Then a new state $s' = (\tau', PC', LC')$ is reached where τ' is the same as τ except that it maps $\tau^{-1}(v_i)$ to v_j and $\tau^{-1}(v_j)$ to v_i , where $\tau^{-1}(v_i)$ and $\tau^{-1}(v_j)$ are, respectively, the preimages of v_i and v_j under τ . Furthermore, LC' is obtained from LC by deleting all gates which are executable by τ' , and PC' is obtained from PC by adding first $SWAP(v_i, v_j)$ and then all the gates just deleted from PC , with the operand qubits changed according to τ' . While most algorithms select one SWAP each time, the A^* algorithm [35] and FiDLS [16] select a sequence of SWAPs. Note that when regarding sequences of SWAPs as legal actions, usually we execute a gate only after the last SWAP is applied.

Finally, the *initial state* s_0 of the QCT process is taken as $(\tau_{ini}, PC_0, LC'_0)$ where PC_0 is the physical circuit consisting of all gates from LC_0 which are executable by τ_{ini} , and LC'_0 the logic circuit obtained by deleting all gates in PC_0 from LC_0 . The *goal states* are those with the associated logical circuit being empty. Note that the associated physical circuit

³In Sec. V we will relax this restriction and allow remote CNOTs to be legal actions.

of any goal state respects the connectivity restraints in AG . The *cost* of a state s depends on the optimisation objective. In this paper, it can be either the total number of auxiliary gates inserted or the depth overhead of the stored physical circuit of s . The aim of QCT is to find a goal state with the minimal cost w.r.t. the particular objective.

Many QCT algorithms in the literature adopt a divide-and-conquer approach in the search process. Starting from the current state $s = (\tau, PC, LC)$, each subtask consists of executing the front layer, the first two layers, or a front section of the circuit. For example, in the A^* algorithm, a shortest path in AG (which corresponds to a sequence of SWAPs) is found which converts τ to a new mapping so that all gates in the first two layers of LC are executable. In [7], Cowtan et al. partition LC into layers and then select the SWAP which can maximally reduce the diameter of the subgraph composed of all pairs of qubits in the current layer. Siraichi et al. [27] decompose LC into sub-circuits each of which leads to an isomorphic subgraph of AG and thus the corresponding embedding can act as a mapping τ' that executes all gates in the sub-circuit. Their algorithm then tries to find a minimal sequence of SWAPs which converts τ to τ' . A similar approach is also adopted in Childs et al. [6].

Unlike the above algorithms, SAHS [34] and FiDLS [16] do not divide the problem into sub-problems. Whenever a mapping is generated, they try to execute as many as possible gates from the logical circuit, no matter which level they are in. SAHS regards each SWAP as a valid action, but when selecting the best SWAP to enforce, it simulates the search process one step further and select the SWAP which has the best consecutive SWAP to apply. In principle, SAHS can go deeper but this will make the algorithm much slower (cf. Fig. 12 for an example). FiDLS regards any sequence with up to k SWAPs as a legal action and selects the sequence which executes the most number of gates per SWAP. In a sense, this means that its search depth can reach k . To ensure the running time is acceptable, in the experiments on Q20, FiDLS chooses k as 3 and introduces various filters to filter out unlike SWAPs.

III. THE PROPOSED MCTS FRAMEWORK

In this section, we describe an MCTS framework for quantum circuit transformation and present a detailed algorithm implementation. The algorithm, called MCTS-Size, aims at finding a goal state which has the minimal number of SWAPs inserted. Shortly in Sec. IV we shall see this can be easily adapted to address other optimisation objectives.

Like general MCTS algorithms, our framework also consists of five major parts: *Selection*, *Expansion*, *Simulation*, *Backpropagation* and *Decision*. However, some significant modifications have been made to cater to the unique characteristics of QCT.

The Monte Carlo search tree for QCT, which is initialised immediately after the algorithm starts, stores all states having been explored during the transformation process. As stated in the previous section, an edge (s', s) connecting node s' and its child s indicates that a SWAP is applied to convert s' to

s . With the aim to minimise the number of inserted gates, we define an immediate, short-term *reward* for each edge and a long-term *value* for each node of the search tree as follows.

The short-term reward $\text{REW}(s', s)$ is the reward collected from the father node s' to the child s , in terms of the number of gates executed by the newly inserted SWAP when this transition is made:

$$\text{REW}(s', s) = \# \text{gates_in_} LC(s') - \# \text{gates_in_} LC(s). \quad (1)$$

The long-term value $\text{VAL}(s)$. To determine the value of a state s , the following two factors are taken into account: (i) the number of inserted SWAPs when transformation of the remaining logical circuit is simulated at s . For efficiency, the simulation is performed on, instead of $LC(s)$ itself, a fixed-sized sub-circuit of $LC(s)$. It is expected that the larger the sub-circuit is for simulation, the better simulated value will be obtained. (ii) the (simulated) value of its best child node and the reward to it collected from s . To be specific,

$$\text{VAL}(s) = \max\{\text{SIM}, \gamma \cdot [\text{REW}(s, s'') + \text{VAL}(s'')]\},$$

where SIM is the simulated value obtained from (i), s'' is the child of s with the maximal value, and γ is a predefined discount factor. In our later implementation, $\text{VAL}(s)$ is initially assigned SIM in the *Simulation* module, and then updated in *Backpropagation*, whenever simulations are performed at a descendant of s . Intuitively, $\text{VAL}(s)$ describes the efficiency of introducing SWAPs (in terms of the average number of executed gates per SWAP) from s , considering both the simulation at itself and the backpropagated one from this child nodes. Obviously, the larger $\text{VAL}(s)$ is, the smaller the number of SWAPs needed to lead s to a goal node, and the ‘better’ s is (compared with its siblings).

In addition to the above definitions, as shown in Fig. 6, our framework differs from traditional MCTS algorithms for game playing in the following ways:

- 1) The simulation is performed on the leaf node selected in the *Selection* module, instead of the child nodes opened in the *Expansion* one. Experimental results on real benchmarks indicate that this achieves a better performance for the QCT problem.
- 2) In game playing, the simulation result can be obtained only when the game is decided. In contrast, the reward of a move in our setting is collected during the execution of CNOT gates from the logic circuit. Consequently, in the *Simulation* module, we simulate only on a sub-circuit of the current logic circuit to improve efficiency.
- 3) We introduce a discount factor, which can be adjusted to better suit the problem setting, when backpropagating the simulated values.

A. Main modules

We now elaborate the five major modules one by one.

Selection. *Selection* is the iterated process to find an appropriate leaf node in the search tree to expand and simulate. It starts from the root node and, in each iteration, evaluates and picks one of the child nodes until a leaf node is reached.

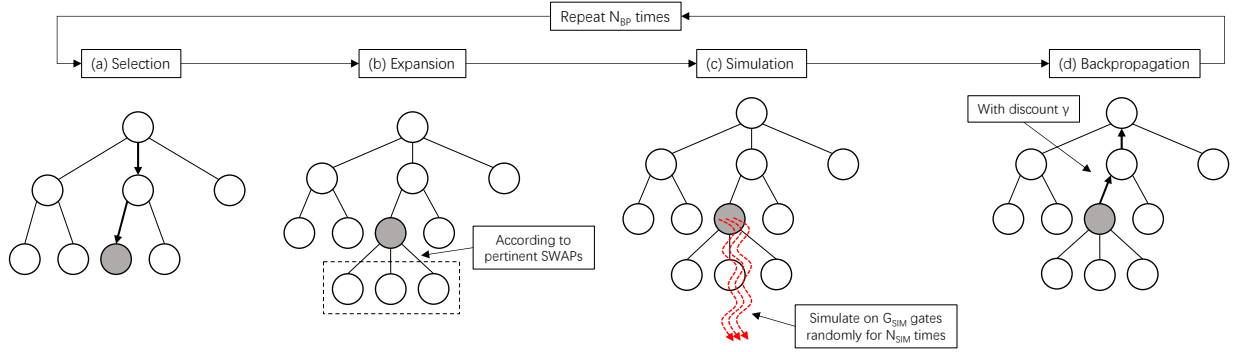


Fig. 6. Overview of the Monte Carlo Tree Search Framework.

The way we evaluate child nodes during *Selection* is critical to the performance of the whole algorithm. On one hand, if we only consider their values, the chance for exploring unpromising nodes will be too low and we can easily get stuck in a local minimum. On the other hand, if we always select nodes with a smaller visit count, the search will be too shallow and thus a large amount of time will be wasted in exploring inferior nodes. To get a balance between these two aspects, the following evaluation formula, similar to the well-known UCT (Upper Confidence Bound 1 applied to trees) [13], is introduced in our implementation to make a balanced evaluation among all child nodes s' of s :

$$\text{REW}(s, s') + \text{VAL}(s') + c \sqrt{\frac{\log \text{VISIT}(s)}{\text{VISIT}(s')}} \quad (2)$$

where c is a pre-defined parameter, and $\text{VISIT}(s)$ is the number of times that s has been visited. Intuitively, the first two terms in Eq. 2 correspond to the exploitation rate and the third the exploration rate in UCT. In each iteration of the *Selection* module, the node which maximises Eq. 2 is selected. The *Selection* module is presented in Alg. 1.

Algorithm 1: Select(\mathcal{T})

input : A Monte Carlo search tree \mathcal{T} .

output: A leaf node to expand and simulate.

```

 $s \leftarrow \text{root}(\mathcal{T});$ 
 $\text{VISIT}(s) \leftarrow \text{VISIT}(s) + 1;$ 
while  $s$  is not a leaf node do
     $s \leftarrow$  the child node  $s'$  of  $s$  that maximises Eq. 2;
     $\text{VISIT}(s) \leftarrow \text{VISIT}(s) + 1;$ 
return  $s;$ 

```

Expansion. The goal of *Expansion* is to open all child nodes of a given leaf node by applying all relevant SWAP operations. Given a logic circuit C and a qubit mapping τ , the set of *pertinent* SWAPs, denoted $\text{SWAP}_{C,\tau}$, is the set of gates $\text{SWAP}(v_i, v_j)$ such that either $\tau^{-1}(v_i)$ or $\tau^{-1}(v_j)$ appears in a gate in the current front layer of C , i.e.,

$$(v_i, v_j) \in E \text{ and } (\tau^{-1}(v_i) \in Q_0 \text{ or } \tau^{-1}(v_j) \in Q_0),$$

where Q_0 is the set of logical qubits that are involved in the gates in $\mathcal{L}_0(C)$. To expand a selected node $s = (\tau, PC, LC)$,

only gates in $\text{SWAP}_{LC,\tau}$ will be applied to generate child nodes. This strategy has been widely used in quantum circuit transformation, see, e.g., [35], [15], [34]. In particular, several variants are introduced in FiDLS [16].

For each pertinent SWAP of s , a new child node s' will be generated. Furthermore, the reward $\text{REW}(s, s')$ is as defined in Eq. 1 and both $\text{VAL}(s')$ and $\text{VISIT}(s')$ are set as 0. The details can be found in Alg. 2.

Algorithm 2: Expand(\mathcal{T}, s)

input : A Monte Carlo search tree \mathcal{T} and node $s = (\tau, PC, LC)$.

```

for all  $\text{SWAP}(v_i, v_j)$  in  $\text{SWAP}_{LC,\tau}$  do
     $\tau' \leftarrow \tau[\tau^{-1}(v_i) \mapsto v_j, \tau^{-1}(v_j) \mapsto v_i];$ 
     $C \leftarrow$  the set of all  $\tau'$ -executable gates in  $LC$ ;
     $LC' \leftarrow LC$  with all gates in  $C$  deleted;
     $PC' \leftarrow PC$  by adding  $\text{SWAP}(u_i, u_j)$  and all gates in  $C$ ;
     $s' \leftarrow (\tau', PC', LC');$ 
     $\text{VAL}(s'), \text{VISIT}(s') \leftarrow 0;$ 
    Add  $s'$  as a child node of  $s$ ;
     $\text{REW}(s, s') \leftarrow$  number of gates in  $C$ ;

```

Simulation. The objective here is to obtain a simulated score, serving as the initial long-term value $\text{VAL}(s)$, of the current state s by simulation. In our implementation, we perform simulation on the first G_{SIM} , a predefined number, gates in the current logical circuit. While almost all existing QCT algorithms can be used for this purpose, for the sake of efficiency, a fast random simulation is designed in Alg. 3.

Given the current state s , let N be, among all N_{SIM} (a predefined number) iterations, the minimal number of SWAP gates we have inserted until all the first G_{SIM} CNOT gates of $LC(s)$ have been executed. Then the initial long-term value of s is defined as

$$\text{VAL}(s) = \gamma^{N/2} \cdot G_{\text{SIM}}, \quad (3)$$

where γ is a predefined discount factor.

We next show how to do random simulation. Let C be a sub-circuit of $LC(s)$ and τ the current mapping. We write

$SWAP_{C,\tau}$ for the set of pertinent SWAPs for C under τ . For any $h \in SWAP_{C,\tau}$, its *impact factor* is defined as

$$IF(h) := f\left(\sum_{g \in \mathcal{L}_0(C)} SCOST(g, \tau) - \sum_{g \in \mathcal{L}_0(C)} SCOST(g, \tau')\right)$$

where τ' is the mapping obtained from τ after applying h and f the scaling function defined as

$$f(x) = \begin{cases} 0, & \text{if } x < 0 \\ 0.001, & \text{if } x = 0 \\ x, & \text{if } x > 0 \end{cases}$$

Furthermore, $SCOST(g, \tau)$ is the *swap cost* of $g = CNOT(q_j, q_k)$ with respect to τ , which is defined to be the shortest distance between the physical qubits $\tau(q_j)$ and $\tau(q_k)$ in the architecture graph. Then, a probability distribution is obtained as follows

$$P(X = h) = \frac{IF(h)}{\sum\{IF(h') \mid h' \in SWAP_{C,\tau}\}}, \quad (4)$$

through which a SWAP operation can be sampled from $SWAP_{C,\tau}$ and used to execute gates from LC . Note that this simulation process will be repeated for N_{SIM} , also a predefined parameter, times to obtain the best score.

Algorithm 3: Simulate(\mathcal{T}, s)

input : A Monte Carlo search tree \mathcal{T} and node $s = (\tau, PC, LC)$.

$N \leftarrow \infty$;

do

$C \leftarrow$ circuit with the first G_{SIM} gates in LC ;

$n \leftarrow 0$; $\tau' \leftarrow \tau$;

while C is not empty **do**

 Sample h from $SWAP_{C,\tau'}$ according to the probability distribution in Eq. 4;

$\tau' \leftarrow \tau'$ by applying h ;

$C \leftarrow C$ with all τ' -executable gates deleted;

$n \leftarrow n + 1$;

if $n < N$ **then**

$N \leftarrow n$;

for N_{SIM} times;

$VAL(s) \leftarrow \gamma^{N/2} \cdot G_{SIM}$;

Another issue which deserves explanation is the way we compute the simulated score (or, the initial value) for state s in Eq. 3. In particular, one may wonder why the exponent is $N/2$ instead of N ? The intuitive meaning of this definition is as follows. Although these G_{SIM} gates are executed in different steps during the simulation, for simplicity, we suppose they are all executed right at the middle point s' which is the $N/2$ -generation son of s . Then the reward collected at the transition to s' from its father is exactly G_{SIM} . Note that every edge along the path from s to the father of s' has zero reward. Thus, we need only backpropagate the reward collected at s' upwards with discount factor γ . This gives the simulated score $\gamma^{N/2} \cdot G_{SIM}$ for s as specified in Eq. 3. Real benchmark experiments also confirm that the current choice performs better than simply letting $VAL(s)$ be the sum of all

(the discounted) rewards collected during the actual execution of these G_{SIM} CNOT gates.

Backpropagation. The *Backpropagation* module updates the values of ancestors of the just simulated node in the search tree. More precisely, the value of node s in the propagated path will be updated as

$$VAL(s) \leftarrow \max\{VAL(s), \gamma \cdot [REW(s, s') + VAL(s')]\}, \quad (5)$$

in which s' is the child node of s on the path. This reflects the intuitive meaning of $VAL(s)$ discussed at the beginning of this section. The implementation is shown in Alg. 4.

Algorithm 4: Backpropagate(\mathcal{T}, s)

input : A Monte Carlo search tree \mathcal{T} and node s .

while $s \neq root(\mathcal{T})$ **do**

$s' \leftarrow$ father node of s ;

$VAL(s') \leftarrow \max\{VAL(s'), \gamma \cdot [REW(s', s) + VAL(s)]\}$;

$s \leftarrow s'$;

Decision. This module, depicted in Alg. 5, decides the best move from the root node rt and updates the search tree with the subtree rooted at the best child node of rt .

Algorithm 5: Decide(\mathcal{T})

input : A Monte Carlo search tree \mathcal{T} .

$rt \leftarrow root(\mathcal{T})$;

$s \leftarrow$ child node of rt with the highest $REW(rt, s) + VAL(s)$;

$\mathcal{T} \leftarrow$ the subtree of \mathcal{T} rooted at s ;

B. Combine Everything Together

Finally, we combine all modules together as in Alg. 6 to form the MCTS framework for QCT. Note that, to ensure the reliability of the *Decision* module, a sufficiently large number (N_{BP} , a predefined parameter) of *Selection*, *Expansion*, *Simulation*, and *Backpropagation*, should be performed to get a good estimation of the values of relevant states.

Due to the stochastic nature of our algorithm, there is a negligible but still positive possibility that at certain iteration of the while loop in Alg. 6, even the best child node derived from the *Decision* module cannot execute any new gate. To guarantee termination in this extreme case, a *fallback* mechanism, which has been widely used in the literature (cf. [6]), is adopted. Specifically, if no CNOTs have been executed after $|V|$ consecutive *Decisions* and the current root node is (τ, PC, LC) , then we choose a CNOT from $\mathcal{L}_0(LC)$ with minimum swap cost with respect to τ , and insert the corresponding SWAP gates to PC so that progress will be made by executing this chosen CNOT.

C. Complexity Analysis

This subsection is devoted to a rough analysis of the complexity of our algorithm. Suppose $AG = (V, E)$ and the

Algorithm 6: Quantum circuit transformation based on Monte Carlo tree search

input : An architecture graph AG , a logical circuit LC , and an initial mapping τ_{ini} .

output: A physical circuit satisfying the connectivity constraints in AG .

$PC \leftarrow$ the circuit consisting of all executable gates in LC under τ_{ini} ;

$LC \leftarrow LC$ with gates in PC deleted;

$s \leftarrow (\tau_{ini}, PC, LC)$;

$VAL(s), VISIT(s) \leftarrow 0$;

$\mathcal{T} \leftarrow$ a search tree with a single (root) node s ;

while $LC(s) \neq \emptyset$ **do**

do

$s \leftarrow \text{Select}(\mathcal{T})$;

$\text{Expand}(\mathcal{T}, s)$;

$\text{Simulate}(\mathcal{T}, s)$;

$\text{Backpropagate}(\mathcal{T}, s)$;

for N_{BP} **times**;

$\text{Decide}(\mathcal{T})$;

$s \leftarrow \text{root}(\mathcal{T})$;

return $PC(s)$

input logical circuit $LC = (Q, C)$. Among the five main modules presented in subsection III-A, the most expensive ones are *Selection*, *Expansion*, and *Simulation*. We analyse their complexity separately as follows.

Selection. The complexity of this module depends on the depth of the search tree. In the worst case, each of the N_{BP} iteration in the **do** loop of Alg. 6 increases the depth by 1. Taking into account the fallback introduced in the last subsection, the depth of the search tree is at most $N_{BP} \cdot |V|$. As each node has at most $|E|$ children, the overall complexity for this module is $O(N_{BP} \cdot |V| \cdot |E|)$.

Expansion. There are at most $|E|$ pertinent SWAP gates available to create new nodes, and for each new one, at most $|C|$ gates need to be checked to see whether they are executable. Thus the time complexity is $O(|E| \cdot |C|)$. Here $|C|$ denotes the number of gates in C .

Simulation. Computing the probability distribution in Eq. 4 takes time $O(|E| \cdot |V|)$. To guarantee termination, the while loop will be aborted if no gates have been executed after $|V|$ consecutive iterations. Hence, the complexity of this module is $O(|E| \cdot |V|^2 \cdot G_{SIM} \cdot N_{SIM})$.

Finally, note that in the worst case, all gates from C are executed by the fallback mechanism which is invoked after every $|V|$ iterations. Hence, the *Sel-Exp-Sim-BP* modules will be run for at most $|C| \cdot |V| \cdot N_{BP}$ times, and the overall time complexity of our algorithm is

$$O(|C| \cdot |V| \cdot N_{BP} \cdot |E| \cdot [N_{BP} \cdot |V| + |C| + |V|^2 \cdot G_{SIM} \cdot N_{SIM}]),$$

or $O(|C| \cdot |V| \cdot |E| \cdot (|C| + |V|^2))$ when the parameters are regarded as constants.

IV. DEPTH OPTIMISATION

QPU's in the NISQ era also suffer from limited coherence time, meaning that the depth of the output physical circuit

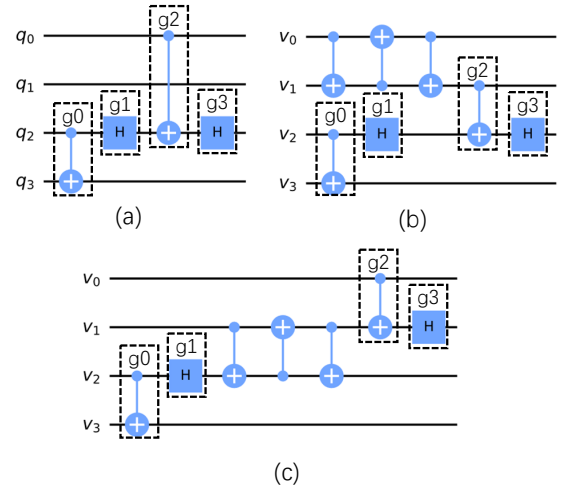


Fig. 7. An input quantum circuit (a) and two functionally equivalent physical circuits, (b) and (c), that are executable on IBM Q20 with the naive initial mapping.

is also an important criterion for optimising the circuit transformation process. In this section, we propose MCTS-Depth, which is adapted from the MCTS-Size algorithm presented in the previous section by introducing two minor changes, to further reduce the depth of the output circuit.

Recall that in MCTS-Size we have removed all single-qubit gates because they have no effect when the QCT objective is to minimise the number of inserted SWAP gates. However, as shown in Example 4, this is not the case as far as circuit depth is concerned. In this paper, we adopt a simple strategy to deal with these gates: whenever an executable CNOT g is removed from the logical circuit and added to the physical circuit in *Expansion*, all single-qubit gates after g and before any other CNOT that directly depends on g will be greedily added to the physical circuit.

Example 4. Suppose the quantum (logical) circuit to be transformed by MCTS-Depth is specified as in Fig. 7(a). Assume that the target QPU is IBM Q20 and we take the initial mapping to be the naive one. As the CNOT g_0 is directly executable, g_0 and the single-qubit gate g_1 are immediately added to the physical circuit. To make g_2 executable, we can insert a SWAP either between physical qubits v_0 and v_1 (cf. Fig. 7(b)) or between v_1 and v_2 (cf. Fig. 7(c)). The depth overhead brought by adding $\text{SWAP}(v_0, v_1)$ and $\text{SWAP}(v_1, v_2)$ are, respectively, 1 and 3, after decomposing each SWAP into 3 CNOTs.

As shown in Example 4, different SWAP gates may incur different depth overheads. Let $s = (\tau, PC, LC)$ be the current state and $s' = (\tau', PC', LC')$ the child state corresponding to some SWAP. As each SWAP is implemented as three consecutive CNOTs, the depth overhead, written $I_{s'}$, is an integer between 0 and 3. That is, a SWAP may incur 0, 1, 2, or 3 extra layers. The precise value of $I_{s'}$ is calculated as the depth difference of PC' and PC , where the executed single-qubit gates are properly added back. Apparently, we prefer SWAPs with smaller $I_{s'}$. This motivates us to replace

the discount factor γ in Eq. 5 for MCTS-Size with $\gamma^{I_{s'}}$ and obtain the following value-update rule for MCTS-Depth:

$$\text{VAL}(s) \leftarrow \max\{\text{VAL}(s), \gamma^{I_{s'}} \cdot [\text{REW}(s, s') + \text{VAL}(s')]\} \quad (6)$$

Another modification is applied to the definition of the initial long-term value of a state s in the simulation process, given in Eq. 3, where it uses N , the minimal number of SWAP gates required during all N_{SIM} simulations, as an important index. Apparently, in order to reduce depth, it is more meaningful to replace N with M , the minimal depth overhead of all N_{SIM} simulations. That is, in MCTS-Depth, Eq. 3 is replaced with

$$\text{VAL}(s) = \gamma^{M/2} \cdot G_{\text{SIM}} \quad (7)$$

and the second last line of Alg. 3 is replaced with

$$\text{VAL}(s) \leftarrow \gamma^{M/2} \cdot G_{\text{SIM}}.$$

It is clear that these modifications do not affect the complexity analysis given in Sec. III-C.

V. INCORPORATING REMOTE CNOT

In above, we have seen how a circuit can be transformed by inserting SWAPs. This is sometimes not desirable as the mapping will change with the inserted SWAPs (cf. Example 5 below). Several transformers (including the current version of `t|ket`) suggest using remote CNOT operations (also known as bridge gates) to execute CNOT gates whose two qubits in the current mapping are not neighbours (i.e., remote). In this section, we show how remote CNOTs can be incorporated into our MCTS-based algorithms.

Let τ be the current mapping and $g = \text{CNOT}(q, q')$. If the two physical qubits $\tau(q)$ and $\tau(q')$ are not neighbours in the target AG, we may replace g with a sequence of CNOT gates, written $\mathcal{R}_\tau(g)$, which are executable and functionally equivalent to g . Fig. 8(b) shows the special case when the distance of $\tau(q)$ and $\tau(q')$ in AG is 2. More general construction can be found in [19].

Example 5. Consider the circuit shown in Fig. 4 (left). Except g_0 , every CNOT in the circuit can be executed by the naive mapping. If only SWAPs are allowed, we need to insert a SWAP to execute g_0 . As a consequence, the mapping is changed and at least one of the other CNOTs are not executable and we need to insert another SWAP, which results in a size overhead of at least six! However, g_0 can be executed by implementing it as a remote CNOT depicted in Fig. 8(b) and, after that, the other CNOTs can be immediately executed, which gives an overhead of three!

To extend our MCTS algorithms with remote CNOT, we need only modify *Expansion* and *Backpropagation*. Starting from a state/node $s = (\tau, PC, LC)$, besides all relevant SWAPs as used in Alg. 2, we also consider all $g = \text{CNOT}(q, q')$ if g is in the first layer of LC and the distance of $\tau(q)$ and $\tau(q')$ in AG is between 2 and some fixed integer d . We then may replace g with a CNOT sequence $\mathcal{R}_\tau(g)$ if desirable. As remote CNOTs and SWAPs may incur different size and depth overheads, a modified value-update rule like

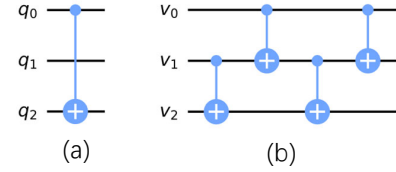


Fig. 8. Take AG to be that of IBM Q20 and the initial mapping τ be naive. (a) A logical circuit with only one gate $\text{CNOT}(q_0, q_2)$. (b) A remote CNOT implementation of $\text{CNOT}(q_0, q_2)$.

Eq. 6 is used during *Backpropagation* if $s' = (\tau', PC', LC')$ is the child node of s derived by a remote CNOT implementation of g . More precisely, for MCTS-Size, $I_{s'}$ is defined as $(|\mathcal{R}_{\tau'}(g)| - 1)/3$. The intuition behind this is that the sub-circuit $\mathcal{R}_{\tau'}(g)$ we used to replace g brings a size overhead of $|\mathcal{R}_{\tau'}(g)| - 1$ in terms of CNOTs, which translates to $(|\mathcal{R}_{\tau'}(g)| - 1)/3$ in terms of SWAPs. For MCTS-Depth, $I_{s'}$ is set as the depth overhead brought by adding gates in $\mathcal{R}_{\tau'}(g)$ to the physical circuit in state s' .

To conclude this section, we point out that the remote CNOT approach does not always give better result than the SWAP-based approach. This is because inserting SWAPs changes the mapping, which is sometimes desirable as the new mapping may execute more later CNOTs. Consider again the circuit in Fig. 4 (left). If the CNOT gate g_3 were applied on q_0 and q_2 , then inserting $\text{SWAP}(v_0, v_1)$ (i.e. three CNOTs) suffices to solve all gates in the circuit, while remote implementation of both g_0 and g_3 would introduce an overhead of six CNOTs. In practice, however, it might not be easy to decide which approach is preferable. Thus we provide both of them as possible choices. In Sec. VI we will evaluate its impact for two AGs.

VI. PROGRAMMING AND BENCHMARKS

To evaluate our approach, we compare it with three state-of-the-art algorithms proposed in the literature [34], [16], [7]. As the choice of initial mappings may sometimes influence the performance of QCT algorithms, to make a fair comparison, we always take the same initial mappings in their original design if available. We use Python as our main programming language and IBM Qiskit [9] as the auxiliary environment to implement our algorithms⁴. For efficiency, the *Simulation* module is implemented in C++. All experimental results reported here are obtained by choosing the best one from 5 trials. Due to space limitations, we only provide summarised results here. Readers are referred to the online Appendix for detailed empirical results.

In our evaluation, we selected a set of 114 benchmark circuits, with a sum of 554,497 gates (including 248,553 CNOTs) and a sum of 303,469 depths, which are taken from [35] and widely used in evaluating circuit transformation algorithms by, e.g., [7], [16], [34], [15].

Our MCTS-based QCT algorithms have a couple of parameters to be determined before actual running:

⁴Source code is available at <https://github.com/BensonZhou1991/Circuit-Transformation-via-Monte-Carlo-Tree-Search>

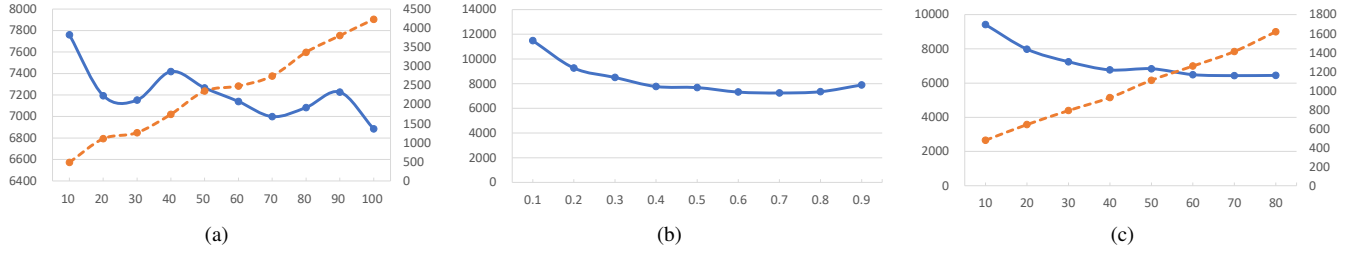


Fig. 9. Evaluation of the performance of MCTS-Size on IBM Q20 for different parameter settings: (a) N_{BP} , (b) γ , and (c) G_{SIM} , where the vertical axes on the left and right in each sub-figure represent the aggregated number of added CNOTs in output circuits (blue lines) and running time (seconds, orange dashed lines), respectively. All data is aggregated from a small set of benchmarks with 11 circuits and 26,676 CNOT gates in total and initial mappings are the same as those used in SAHS [34].

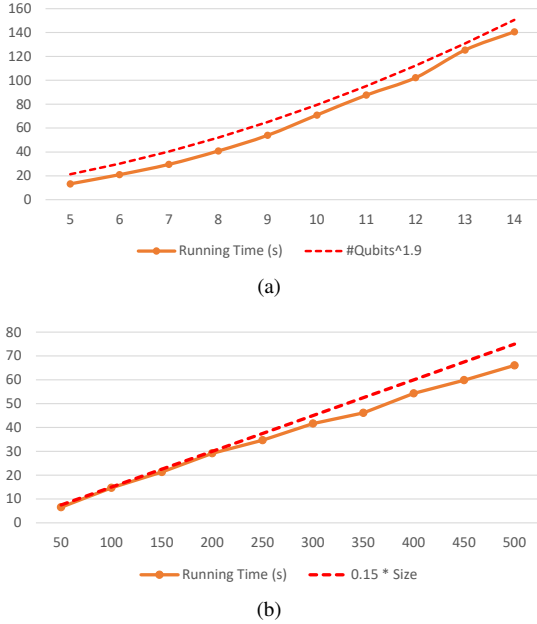


Fig. 10. Evaluations of the performance of MCTS-Size on IBM Q20 by comparing the average running time (seconds, orange line) with (a): number of logical qubits, and (b): number of CNOTs of the input circuits, where each circuit in (a) contains 500 CNOTs and each circuit in (b) has 10 qubits, and each data point denotes the average value of 10 randomly generated quantum circuits with naive initial mappings.

- N_{BP} (repeated times for the *Sel-Exp-Sim-BP* modules before each *Decision*),
- c (the exploration parameter used in Eq. 2),
- G_{SIM} (the size of sub-circuit used in simulation),
- N_{SIM} (the number of simulations),
- γ (the discount ratio), and
- d (the maximum distance allowed for remote CNOT).

To help determine these parameters for IBM Q20, we selected a small subset of 11 benchmark circuits, which contains in total 26,676 CNOTs. To get a good balance between performance and running time, we empirically set

$$N_{BP} = c = 20, G_{SIM} = 30, N_{SIM} = 500, \text{ and } \gamma = 0.7.$$

We adopt the same parameter setting for the other proposed algorithms, and set $d = 2$ for MCTS-Size and MCTS-Depth.

We have shown in Sec. III-C that our algorithm runs in time polynomial in all relevant parameters. To further demonstrate the running time in practice, we randomly generate two sets of

10 quantum circuits. In one set, each circuit has 500 CNOTs, and the number of logical qubits ranges from 5 to 14. In the other, each circuit has 10 qubits, and the number of CNOTs ranges from 50 to 500. We transform all these circuits via MCTS-Size on IBM Q20, and record the average running time for each circuit set. As shown in Fig. 10, the real time cost is roughly the 1.9th power in the number of qubits and linear (with slope being about 0.15) in the number of CNOTs, indicating that our algorithm is practically scalable.

Now we compare MCTS-Size with SAHS [34], FiDLS [16], and t|ket⟩[7] on IBM Q20 over the 114 benchmark circuits. The results are summarised in Table I, where the ‘improvement’ is defined as $(n_{comp} - n_{ours})/n_{comp}$, with n_{comp} and n_{ours} being the total numbers of CNOT gates added by the compared algorithm and ours, respectively, in transforming the 114 circuits. A similar definition for ‘Improvement’ is used in the rest of the paper.

TABLE I
SUMMARISED RESULTS FOR A LARGE BENCHMARK SET WITH 114 CIRCUITS AND 248,553 CNOTS IN TOTAL, WHERE COLUMNS 2 & 3 REPRESENT AGGREGATED NUMBERS OF ADDED CNOTS OBTAINED FROM OTHER METHODS AND MCTS-Size WHEN USING THEIR INITIAL MAPPINGS, RESPECTIVELY.

	CNOT Added Others	CNOT Added MCTS-Size	Improvement
SAHS	116487	73758	36.68%
Topg. FiDLS	107406	74763	30.39%
Weig. FiDLS	105645	75126	28.89%
t ket⟩	238170	77544	59.24%

From Table I, we can see that MCTS-Size achieves a conspicuous improvement of 36.68% on average when compared with SAHS (by using the same initial mappings as SAHS). In [16], two techniques for initial mappings, topgraph (topg.) and weighted graph (weig.), are proposed with FiDLS. Our algorithm has a consistent improvement, 30.39% for the topgraph initial mappings and 28.89% for the weighted graph ones. The version of t|ket⟩ we compare with is 0.7.0.⁵ As the initial mappings of t|ket⟩ are not directly available, we use naive mappings as the initial mappings in the experiments. For fair and pure comparison of the routing abilities, we also disabled the postmapping optimisation of t|ket⟩. As can be seen from the last row of Table I, the gate overhead of t|ket⟩ is above 3 times of ours (also with naive initial mappings). It is worth noting that, on this benchmark set, MCTS-Size still

⁵<https://cqcl.github.io/pytket/build/html/index.html>

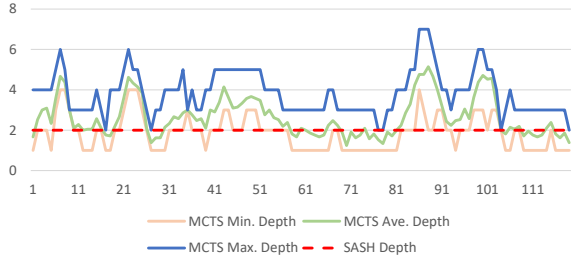


Fig. 11. Search depth (for *Selection* before each *Decision*) of MCTS-Size for circuit 'misex1_241'. The horizontal and vertical axes represent rounds for *Decision* and search depth, respectively.

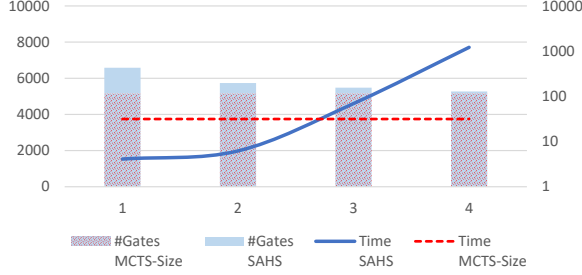


Fig. 12. The benefit brought by increasing the search depth in SAHS [34] for circuit 'misex1_241'. The horizontal axis and vertical axes on the left and right represent search depth, number of gates in the output circuit and running time (seconds), respectively.

performs well even with naive initial mappings; the overhead compared with the best result is only 5.13% (77,544 vs. 73,758).

For MCTS-Size, we also record the search depth for each use of the *Selection* module and calculate the minimum, average, and maximum depth before each *Decision* process. As shown in Fig. 11, the maximum depth can easily exceed that of SAHS [34], which is set to 2. Actually, in most of the time it is more than 3, meaning that our algorithm has better ability of exploring the unknown state. Note that it is claimed in [34] that the size of output physical circuits can be further decreased by increasing the search depth, with the cost of more time consumption. Fig. 12 depicts a comparison of the output circuit size as well as the running time of MCTS-Size and SAHS on the example circuit 'misex1_241' with 4,813 gates, where for SAHS, the search depth varies from 1 to 4. It shows that MCTS-Size outperforms SAHS in the output circuit size even when the search depth of SAHS is set to 4. However, in this case, the running time of SAHS is over 20 minutes, while MCTS-Size only needs 31 seconds.

Now we compare MCTS-Depth with both MCTS-Size and $t|ket\rangle$ on the benchmark set in terms of the total depth overhead. As the initial mappings used by $t|ket\rangle$ are not directly available, we adopt the naive mapping as the initial mapping for all three algorithms. It is surprise that on IBM Q20 the initial mappings selected by $t|ket\rangle$ are, in average, not better than the naive mappings (238,170 vs. 237,471 added CNOTs and 238,051 vs. 236,312 added depths). As can be seen from Table II, MCTS-Depth is able to improve the depth performance steadily for both tested AGs when compared to MCTS-Size, which confirms the utility of our modifications

in Sec. IV. We note that the improvements of Alg. X against Alg. Y in Table II are calculated as $(n_Y - n_X)/n_Y$ with n_Y (n_X , resp.) being either the sum of the added CNOTs or the sum of the added depths by Alg. Y (Alg. X, resp.). When compared with $t|ket\rangle$, for IBM Q20, both MCTS-Size and MCTS-Depth have a great advantage, with about 75% and 84% improvement; for Grid 5×4 , however, their advantages are not so remarkable. The main reason is perhaps due to the fact that IBM Q20 supports more qubit connections (and has a smaller diameter) than Grid 5×4 , which enables the MCTS-based algorithms to find a good solution without going much deeper for IBM Q20. Another reason may be that $t|ket\rangle$ performs really well on grid-like AGs.

Finally, we discuss the improvement brought by introducing remote CNOT. We empirically evaluated the impact of remote CNOT in our MCTS-based algorithms and $t|ket\rangle$. The results are summarised in Table II, where for an algorithm A, A+r denotes the algorithm with remote CNOT enabled. For IBM Q20, the improvements brought by introducing remote CNOT are almost negligible, and sometimes even degraded. For Grid 5×4 , however, the improvements are quite significant. Compared to $t|ket\rangle$, our algorithms have gained an improvement of 28% in size (MCTS-Size-r) and an improvement of 42% in depth (MCTS-Depth-r), while $t|ket\rangle$ -r has a 4% improvement in size and a 14% improvement in depth.

TABLE II
SUMMARISED RESULTS OF THE PROPOSED ALGORITHMS AND $t|ket\rangle$ OVER THE LARGE BENCHMARK SET (WITH TOTAL DEPTHS 303,469) ON IBM Q20 AND GRID 5×4 WITH NAIVE INITIAL MAPPINGS, WHERE A+R DENOTES THE ALGORITHM A WITH REMOTE CNOT ENABLED. COLUMNS 5 & 6 REPRESENT, RESPECTIVELY, THE SIZE AND DEPTH IMPROVEMENT COMPARED TO $t|ket\rangle$.

AG	Method	CNOT Added	Depth Added	Size Imp.	Depth Imp.
IBM Q20	$t ket\rangle$	237471	236312	-	-
	$t ket\rangle$ +r	273420	238661	-15.14%	-0.99%
	MCTS-Size	79743	58602	66.42%	75.20%
	MCTS-Size+r	79275	59857	66.62%	74.67%
	MCTS-Depth	151530	37794	36.19%	84.01%
	MCTS-Depth+r	147972	37138	37.69%	84.28%
Grid 5×4	$t ket\rangle$	383409	368109	-	-
	$t ket\rangle$ +r	367815	314148	4.07%	14.66%
	MCTS-Size	356091	359240	7.13%	2.41%
	MCTS-Size+r	275274	263811	28.20%	28.33%
	MCTS-Depth	514311	292050	-34.14%	20.66%
	MCTS-Depth+r	392349	211421	-2.33%	42.57%

VII. CONCLUSION

In this paper, an MCTS framework is proposed for the quantum circuit transformation problem, which aims at minimising either the size or the depth overhead to transform an ideal logical circuit to a physical one executable on a QPU with connectivity constraints. For this purpose, a scoring mechanism (cf. Eqs 5 and 6) is designed which takes into account both the short-term reward of introducing a SWAP and a long-term value obtained by random simulations. Furthermore, when backpropagating rewards collected by states to their ancestors, a discount factor is introduced to guide the algorithm towards a cheapest path to a goal state. The MCTS-based algorithms, viz., MCTS-Size and MCTS-Depth, run in polynomial time with respect to all relevant parameters. With six parameters,

they are very flexible in meeting different optimisation objectives, can stop whenever a preassigned resource limit is reached, and search much deeper than existing algorithms. Empirical results on extensive realistic circuits on IBM Q20 confirmed that MCTS-Size (MCTS-Depth, resp.) can reduce, in average, the CNOT (depth, resp.) overhead by at least 75% (84%, resp.) when compared with $t|ket\rangle$, an industrial level product.

Recently, Tan and Cui [29] proposed a random circuit library QUEKO for evaluating the optimality of quantum circuit transformers, which contains circuits with known optimal depth overhead. We evaluated MCTS-Depth on QUEKO and the results show a total score of 2.88 (meaning the ratio of the total depths of the output and input circuits), which is, though better than that of $t|ket\rangle$ (3.76), is still too far from the optimal ratio, viz. 1. This is partially due to that we used naive initial mappings, instead of the optimal mappings, e.g., those found by subgraph isomorphism [16]. On the other hand, it suggests that there is still much room to improve the implementation of our algorithms. This is the first problem we intend to attack for future studies. Second, parameters presented in our algorithms are QPU-dependent, and a careful study of their correlation may provide a better insight on how to choose them in practice. Third, more objectives, e.g., fidelity and error rate, should be included in evaluating the quality of output physical circuits. Last but not least, it is promising to develop a parallelised implementation of our MCTS-based algorithms in a multi-thread way, where hundreds or thousands computational processes can run in parallel and share the same memory. The success implementation of this parallelised MCTS framework could help us get even better results (by going deeper) more quickly.

VIII. ACKNOWLEDGMENTS

This work was supported by the National Key R&D Program of China (Grant No. 2018YFA0306704) and the Australian Research Council (Grant No. DP180100691).

APPENDIX

For detailed empirical results please see the appendix.

REFERENCES

- [1] F. Arute, K. Arya, R. Babbush, D. Bacon, J. C. Bardin, R. Barends, R. Biswas, S. Boixo, F. G. Brandao, D. A. Buell, et al. Quantum supremacy using a programmable superconducting processor. *Nature*, 574(7779):505–510, 2019.
- [2] A. Barenco, C. H. Bennett, R. Cleve, D. P. DiVincenzo, N. Margolus, P. Shor, T. Sleator, J. A. Smolin, and H. Weinfurter. Elementary gates for quantum computation. *Physical Review A*, 52(5):3457, 1995.
- [3] K. E. Booth, M. Do, J. C. Beck, E. Rieffel, D. Venturelli, and J. Frank. Comparing and integrating constraint programming and temporal planning for quantum circuit compilation. In *Twenty-Eighth International Conference on Automated Planning and Scheduling*, 2018.
- [4] C. B. Browne, E. Powley, D. Whitehouse, S. M. Lucas, P. I. Cowling, P. Rohlfshagen, S. Tavener, D. Perez, S. Samothrakis, and S. Colton. A survey of monte carlo tree search methods. *IEEE Transactions on Computational Intelligence and AI in games*, 4(1):1–43, 2012.
- [5] G. M. J. Chaslot, M. H. Winands, H. J. V. D. HERIK, J. W. Uiterwijk, and B. Bouzy. Progressive strategies for monte-carlo tree search. *New Mathematics and Natural Computation*, 4(03):343–357, 2008.
- [6] A. M. Childs, E. Schoute, and C. M. Unsal. Circuit transformations for quantum architectures. In *14th Conference on the Theory of Quantum Computation, Communication and Cryptography*, 2019.
- [7] A. Cowtan, S. Dilkes, R. Duncan, A. Krajenbrink, W. Simmons, and S. Sivarajah. On the qubit routing problem. In *14th Conference on the Theory of Quantum Computation, Communication and Cryptography*, 2019.
- [8] A. A. de Almeida, G. W. Dueck, and A. C. da Silva. Finding optimal qubit permutations for IBM’s quantum computer architectures. In *Proceedings of the 32nd Symposium on Integrated Circuits and Systems Design*, pages 1–6, 2019.
- [9] G. A. et al. Qiskit: An open-source framework for quantum computing, 2019.
- [10] W. Finigan, M. Cubeddu, T. Lively, J. Flick, and P. Narang. Qubit allocation for noisy intermediate-scale quantum computers. *arXiv preprint arXiv:1810.08291*, 2018.
- [11] T. Häner, D. S. Steiger, K. Svore, and M. Troyer. A software methodology for compiling quantum programs. *Quantum Science and Technology*, 3(2):020501, 2018.
- [12] T. Itoko, R. Raymond, T. Imamichi, A. Matsuo, and A. W. Cross. Quantum circuit compilers using gate commutation rules. In *Proceedings of the 24th Asia and South Pacific Design Automation Conference*, pages 191–196. ACM, 2019.
- [13] L. Kocsis and C. Szepesvári. Bandit based monte-carlo planning. In *15th European Conference on Machine Learning*, pages 282–293. Springer, 2006.
- [14] L. Lao, D. M. Manzano, H. van Someren, I. Ashraf, and C. G. Almudever. Mapping of quantum circuits onto nisq superconducting processors. *Quantum*, 2:3, 2019.
- [15] G. Li, Y. Ding, and Y. Xie. Tackling the qubit mapping problem for NISQ-era quantum devices. In *Proceedings of the Twenty-Fourth International Conference on Architectural Support for Programming Languages and Operating Systems*, pages 1001–1014. ACM, 2019.
- [16] S. Li, X. Zhou, and Y. Feng. Qubit mapping based on subgraph isomorphism and filtered depth-limited search. *IEEE Transactions on Computers*, accepted.
- [17] A. Lye, R. Wille, and R. Drechsler. Determining the minimal number of swap gates for multi-dimensional nearest neighbor quantum circuits. In *The 20th Asia and South Pacific Design Automation Conference*, pages 178–183. IEEE, 2015.
- [18] P. Murali, J. M. Baker, A. Javadi-Abhari, F. T. Chong, and M. Martonosi. Noise-adaptive compiler mappings for noisy intermediate-scale quantum computers. In *Proceedings of the Twenty-Fourth International Conference on Architectural Support for Programming Languages and Operating Systems*, pages 1015–1029. ACM, 2019.
- [19] B. Nash, V. Gheorghiu, and M. Mosca. Quantum circuit optimizations for NISQ architectures. *Quantum Science and Technology*, 5(2):025010, 2020.
- [20] M. A. Nielsen and I. Chuang. *Quantum computation and quantum information*. Cambridge University Press, 2002.
- [21] S. Nishio, Y. Pan, T. Satoh, H. Amano, and R. V. Meter. Extracting success from ibm’s 20-qubit machines using error-aware compilation. *ACM Journal on Emerging Technologies in Computing Systems (JETC)*, 16(3):1–25, 2020.
- [22] A. Paler. On the influence of initial qubit placement during NISQ circuit compilation. In *International Workshop on Quantum Technology and Optimization Problems*, pages 207–217. Springer, 2019.
- [23] M. Saeedi, R. Wille, and R. Drechsler. Synthesis of quantum circuits for linear nearest neighbor architectures. *Quantum Information Processing*, 10(3):355–377, 2011.
- [24] V. V. Shende, S. S. Bullock, and I. L. Markov. Synthesis of quantum-logic circuits. *IEEE Transactions on Computer-Aided Design of Integrated Circuits and Systems*, 25(6):1000–1010, 2006.
- [25] D. Silver, A. Huang, C. J. Maddison, A. Guez, L. Sifre, G. Van Den Driessche, J. Schrittwieser, I. Antonoglou, V. Panneershelvam, M. Lanctot, et al. Mastering the game of go with deep neural networks and tree search. *Nature*, 529(7587):484, 2016.
- [26] D. Silver, J. Schrittwieser, K. Simonyan, I. Antonoglou, A. Huang, A. Guez, T. Hubert, L. Baker, M. Lai, A. Bolton, et al. Mastering the game of go without human knowledge. *Nature*, 550(7676):354–359, 2017.
- [27] M. Y. Siraichi, V. F. dos Santos, C. Collange, and F. M. Q. Pereira. Qubit allocation as a combination of subgraph isomorphism and token swapping. *Proc. ACM Program. Lang.*, 3(OOPSLA):120:1–120:29, 2019.

- [28] M. Y. Siraichi, V. F. d. Santos, S. Collange, and F. M. Q. Pereira. Qubit allocation. In *Proceedings of the 2018 International Symposium on Code Generation and Optimization*, pages 113–125. ACM, 2018.
- [29] B. Tan and J. Cong. Optimality study of existing quantum computing layout synthesis tools. *IEEE Transactions on Computers*, accepted.
- [30] D. Venturelli, M. Do, E. Rieffel, and J. Frank. Compiling quantum circuits to realistic hardware architectures using temporal planners. *Quantum Science and Technology*, 3(2):025004, 2018.
- [31] D. Venturelli, M. Do, E. G. Rieffel, and J. Frank. Temporal planning for compilation of quantum approximate optimization circuits. In *Twenty-Sixth International Joint Conference on Artificial Intelligence*, pages 4440–4446, 2017.
- [32] C. Zhang, Y. Chen, Y. Jin, W. Ahn, Y. Zhang, and E. Z. Zhang. A depth-aware swap insertion scheme for the qubit mapping problem. *arXiv preprint arXiv:2002.07289*, 2020.
- [33] X. Zhou, Y. Feng, and S. Li. A monte carlo tree search framework for quantum circuit transformation. In *2020 IEEE/ACM International Conference on Computer-Aided Design (ICCAD)*, pages 1–7. IEEE, 2020.
- [34] X. Zhou, S. Li, and Y. Feng. Quantum circuit transformation based on simulated annealing and heuristic search. *IEEE Transactions on Computer-Aided Design of Integrated Circuits and Systems*, 39(12):4683–4694, 2020.
- [35] A. Zulehner, A. Paller, and R. Wille. An efficient methodology for mapping quantum circuits to the ibm qx architectures. *IEEE Transactions on Computer-Aided Design of Integrated Circuits and Systems*, 38(7):1226–1236, 2018.

TABLE III: Comparison of MCTS-Size with SAHS [34] on IBM Q20.

Circuit Name	Input CNOT	CNOT Added SAHS	CNOT Added MCTS-Size	Improvement
graycode6_47	5	0	0	0.0%
xor5_254	5	0	0	0.0%
ex1_226	5	0	0	0.0%
4gt11_84	9	0	0	0.0%
ex-1_166	9	0	0	0.0%
ham3_102	11	0	0	0.0%
4mod5-v0_20	10	0	0	0.0%
4mod5-v1_22	11	0	0	0.0%
mod5d1_63	13	0	0	0.0%
4gt11_83	14	0	0	0.0%
4gt11_82	18	3	3	0.0%
rd32-v0_66	16	0	0	0.0%
mod5mils_65	16	0	0	0.0%
4mod5-v0_19	16	0	0	0.0%
rd32-v1_68	16	0	0	0.0%
alu-v0_27	17	6	6	0.0%
3_17_13	17	0	0	0.0%
4mod5-v1_24	16	0	0	0.0%
alu-v1_29	17	6	6	0.0%
alu-v1_28	18	6	6	0.0%
alu-v3_35	18	6	6	0.0%
alu-v2_33	17	6	6	0.0%
alu-v4_37	18	6	6	0.0%
miller_11	23	0	0	0.0%
decod24-v0_38	23	0	0	0.0%
alu-v3_34	24	6	6	0.0%
decod24-v2_43	22	0	0	0.0%
mod5d2_64	25	12	12	0.0%
4gt13_92	30	0	0	0.0%
4gt13-v1_93	30	0	0	0.0%
one-two-three-v2_100	32	9	9	0.0%
4mod5-v1_23	32	9	9	0.0%
4mod5-v0_18	31	9	9	0.0%
one-two-three-v3_101	32	6	6	0.0%
4mod5-bdd_287	31	6	6	0.0%
decod24-bdd_294	32	15	15	0.0%
4gt5_75	38	15	15	0.0%
alu-v0_26	38	9	9	0.0%
rd32_270	36	12	12	0.0%
alu-bdd_288	38	24	15	37.5%
decod24-v1_41	38	15	12	20.0%
4gt5_76	46	15	15	0.0%
4gt13_91	49	15	15	0.0%
4gt13_90	53	27	21	22.2%
alu-v4_36	51	15	15	0.0%
4gt5_77	58	9	9	0.0%
one-two-three-v1_99	59	12	12	0.0%
rd53_138	60	27	27	0.0%
one-two-three-v0_98	65	24	24	0.0%
4gt10-v1_81	66	27	21	22.2%
decod24-v3_45	64	15	15	0.0%
aj-e11_165	69	18	18	0.0%
4mod7-v0_94	72	12	12	0.0%
alu-v2_32	72	15	15	0.0%

TABLE III: Comparison of MCTS-Size with SAHS [34] on IBM Q20.

Circuit Name	Input CNOT	CNOT Added SAHS	CNOT Added MCTS-Size	Improvement
4mod7-v1_96	72	18	18	0.0%
cnt3-5_179	85	15	9	40.0%
mod10_176	78	24	24	0.0%
4gt4-v0_80	79	24	24	0.0%
4gt12-v0_88	86	21	21	0.0%
0410184_169	104	12	12	0.0%
4_49_16	99	36	27	25.0%
4gt12-v1_89	100	24	15	37.5%
4gt4-v0_79	105	12	9	25.0%
hwb4_49	107	33	30	9.1%
4gt4-v0_78	109	15	15	0.0%
mod10_171	108	24	24	0.0%
4gt12-v0_87	112	6	6	0.0%
4gt12-v0_86	116	9	9	0.0%
4gt4-v0_72	113	42	18	57.1%
4gt4-v1_74	119	78	30	61.5%
mini-alu_167	126	33	33	0.0%
one-two-three-v0_97	128	66	39	40.9%
rd53_135	134	54	54	0.0%
ham7_104	149	81	60	25.9%
decod24-enable_126	149	87	54	37.9%
mod8-10_178	152	21	21	0.0%
4gt4-v0_73	179	42	42	0.0%
ex3_229	175	18	18	0.0%
mod8-10_177	196	39	36	7.7%
alu-v2_31	198	54	48	11.1%
C17_204	205	96	60	37.5%
rd53_131	200	90	51	43.3%
alu-v2_30	223	45	45	0.0%
mod5adder_127	239	51	51	0.0%
rd53_133	256	105	84	20.0%
majority_239	267	84	60	28.6%
ex2_227	275	96	78	18.7%
cm82a_208	283	84	84	0.0%
sf_276	336	24	24	0.0%
sf_274	336	24	24	0.0%
con1_216	415	192	102	46.9%
rd53_130	448	171	132	22.8%
f2_232	525	213	105	50.7%
rd53_251	564	204	147	27.9%
hwb5_53	598	174	159	8.6%
radd_250	1405	669	441	34.1%
rd73_252	2319	1065	627	41.1%
cycle10_2_110	2648	1296	759	41.4%
hwb6_56	2952	1104	813	26.4%
cm85a_209	4986	2337	1278	45.3%
rd84_253	5960	3246	1950	39.9%
root_255	7493	3525	2082	40.9%
mlp4_245	8232	4116	2670	35.1%
urf2_277	10066	5934	4470	24.7%
sym9_148	9408	2172	1146	47.2%
hwb7_59	10681	4602	2769	39.8%
clip_206	14772	6843	4596	32.8%
sym9_193	15232	6441	4104	36.3%

TABLE III: Comparison of MCTS-Size with SAHS [34] on IBM Q20.

Circuit Name	Input CNOT	CNOT Added SAHS	CNOT Added MCTS-Size	Improvement
dist_223	16624	6936	4719	32.0%
sao2_257	16864	7827	4515	42.3%
urf5_280	23764	13065	8721	33.2%
urf1_278	26692	15678	11040	29.6%
sym10_262	28084	11697	6636	43.3%
hwb8_113	30372	14976	8127	45.7%
summary	248553	116487	73758	36.7%

TABLE IV: Comparison of MCTS-Size to FiDLS [16] based on various initial mappings including Naive, Topgraph (topgr.) [16] and Weighted graph (wgtgr.) [16] on IBM Q20.

Circuit Name	Input CNOT	CNOT Added Naive MCTS	CNOT Added Topg. FiDLS	CNOT Added Topg. MCTS	CNOT Added Weig. FiDLS	CNOT Added Topg. MCTS
graycode6_47	5	9	0	0	0	0
xor5_254	5	15	0	0	0	0
ex1_226	5	15	0	0	0	0
4gt11_84	9	12	0	0	0	0
ex-1_166	9	6	0	0	0	0
ham3_102	11	6	0	0	0	0
4mod5-v0_20	10	9	0	0	0	0
4mod5-v1_22	11	9	0	0	0	0
mod5d1_63	13	12	0	0	0	0
4gt11_83	14	12	0	0	0	0
4gt11_82	18	15	3	3	3	3
rd32-v0_66	16	12	0	0	0	0
mod5mils_65	16	18	0	0	0	0
4mod5-v0_19	16	15	0	0	0	0
rd32-v1_68	16	12	0	0	0	0
alu-v0_27	17	15	9	6	6	9
3_17_13	17	6	0	0	0	0
4mod5-v1_24	16	15	0	0	0	0
alu-v1_29	17	18	9	6	6	9
alu-v1_28	18	15	9	6	6	9
alu-v3_35	18	15	9	6	6	9
alu-v2_33	17	15	9	6	6	6
alu-v4_37	18	15	9	6	6	9
miller_11	23	6	0	0	0	0
decod24-v0_38	23	12	0	0	0	0
alu-v3_34	24	15	9	6	6	12
decod24-v2_43	22	12	0	0	0	0
mod5d2_64	25	21	18	9	9	12
4gt13_92	30	21	0	0	0	0
4gt13-v1_93	30	24	0	0	0	0
one-two-three-v2_100	32	24	9	9	9	9
4mod5-v1_23	32	24	9	15	21	9
4mod5-v0_18	31	24	9	12	12	9
one-two-three-v3_101	32	27	15	9	18	9
4mod5-bdd_287	31	21	6	12	18	6
decod24-bdd_294	32	21	15	15	27	12
4gt5_75	38	24	9	9	12	15
alu-v0_26	38	27	12	9	9	12
rd32_270	36	27	18	18	24	12

TABLE IV: Comparison of MCTS-Size to FiDLS [16] based on various initial mappings including Naive, Topgraph (topgr.) [16] and Weighted graph (wtgr.) [16] on IBM Q20.

Circuit Name	Input CNOT	CNOT Added Naive MCTS	CNOT Added Topg. FiDLS	CNOT Added Topg. MCTS	CNOT Added Weig. FiDLS	CNOT Added Topg. MCTS
alu-bdd_288	38	27	24	15	15	24
decod24-v1_41	38	30	3	15	21	3
4gt5_76	46	27	21	24	36	15
4gt13_91	49	27	6	6	6	6
4gt13_90	53	30	9	9	9	9
alu-v4_36	51	30	6	21	15	6
4gt5_77	58	24	9	18	18	9
one-two-three-v1_99	59	30	24	27	33	15
rd53_138	60	33	30	30	42	24
one-two-three-v0_98	65	39	18	27	27	18
4gt10-v1_81	66	33	15	18	18	15
decod24-v3_45	64	39	15	24	24	15
aj-e11_165	69	33	33	21	36	18
4mod7-v0_94	72	42	12	27	27	12
alu-v2_32	72	27	15	21	45	15
4mod7-v1_96	72	33	21	21	21	27
cnt3-5_179	85	63	3	15	30	3
mod10_176	78	36	15	24	24	15
4gt4-v0_80	79	48	15	12	39	21
4gt12-v0_88	86	48	21	12	15	18
0410184_169	104	72	6	24	27	6
4_49_16	99	42	18	30	30	21
4gt12-v1_89	100	36	57	12	18	27
4gt4-v0_79	105	54	12	9	12	9
hwb4_49	107	42	36	39	42	30
4gt4-v0_78	109	60	15	15	15	15
mod10_171	108	42	39	27	27	33
4gt12-v0_87	112	60	6	6	6	6
4gt12-v0_86	116	63	9	9	9	9
4gt4-v0_72	113	60	45	36	39	27
4gt4-v1_74	119	72	39	27	27	24
mini-alu_167	126	48	30	33	33	30
one-two-three-v0_97	128	57	42	51	78	36
rd53_135	134	81	60	66	84	60
ham7_104	149	51	48	39	42	36
decod24-enable_126	149	69	66	51	63	42
mod8-10_178	152	33	69	24	33	48
4gt4-v0_73	179	66	99	42	42	87
ex3_229	175	42	24	24	81	15
mod8-10_177	196	57	123	42	78	54
alu-v2_31	198	81	78	60	90	57
C17_204	205	81	111	72	84	63
rd53_131	200	78	63	75	78	33
alu-v2_30	223	84	60	57	54	51
mod5adder_127	239	69	84	51	81	81
rd53_133	256	84	60	90	174	39
majority_239	267	96	66	84	105	93
ex2_227	275	93	78	90	108	72
cm82a_208	283	93	117	78	105	60
sf_276	336	60	36	24	36	24
sf_274	336	45	30	24	36	69
con1_216	415	138	273	111	153	162

TABLE IV: Comparison of MCTS-Size to FiDLS [16] based on various initial mappings including Naive, Topgraph (topgr.) [16] and Weighted graph (wtgr.) [16] on IBM Q20.

Circuit Name	Input CNOT	CNOT Added Naive MCTS	CNOT Added Topg. FiDLS	CNOT Added Topg. MCTS	CNOT Added Weig. FiDLS	CNOT Added Topg. MCTS
rd53_130	448	126	267	144	207	129
f2_232	525	114	336	111	126	117
rd53_251	564	159	201	144	195	165
hwb5_53	598	174	207	171	204	156
radd_250	1405	453	633	474	567	435
rd73_252	2319	813	1062	630	852	825
cycle10_2_110	2648	891	1125	954	1290	912
hwb6_56	2952	825	1077	783	1026	834
cm85a_209	4986	1479	2073	1449	2091	1140
rd84_253	5960	1959	2952	1995	2841	2055
root_255	7493	2442	2928	2196	3099	2013
mlp4_245	8232	2811	4275	2838	4146	2844
urf2_277	10066	4551	6285	4605	6267	4560
sym9_148	9408	1206	1947	1311	2166	1131
hwb7_59	10681	2826	3684	2904	3846	2805
clip_206	14772	4773	6762	4677	6834	4764
sym9_193	15232	3783	5481	3855	6462	4020
dist_223	16624	4560	7470	4764	6582	4857
sao2_257	16864	4899	7596	4386	6756	4749
urf5_280	23764	8721	11988	8946	11679	8916
urf1_278	26692	10824	13872	10749	13809	10548
sym10_262	28084	7500	11490	6633	10623	7284
hwb8_113	30372	8226	11295	8073	11382	7989
Summary	248553	77544	107406	74763	105645	75126

TABLE V: Comparison of MCTS-Depth with $t|ket\rangle$ [7] on IBM Q20 with naive initial mappings.

Circuit Name	Input Gates	Input Depth	Gates Added Pytket	Depth Added Pytket	Gates Added MCTS-Depth	Depth Added MCTS-Depth	Improvement
graycode6_47	5	5	9	3	9	3	0.0%
xor5_254	7	5	15	10	18	5	50.0%
ex1_226	7	5	15	10	18	5	50.0%
4gt11_84	18	11	12	10	27	8	20.0%
ex-1_166	19	12	9	10	12	6	40.0%
ham3_102	20	13	12	13	18	8	38.5%
4mod5-v0_20	20	12	15	13	9	3	76.9%
4mod5-v1_22	21	12	15	17	21	9	47.1%
mod5d1_63	22	13	24	24	21	6	75.0%
4gt11_83	23	16	18	19	15	4	78.9%
4gt11_82	27	20	30	31	33	6	80.6%
rd32-v0_66	34	20	24	26	15	6	76.9%
mod5mils_65	35	21	30	27	21	6	77.8%
4mod5-v0_19	35	21	30	29	24	5	82.8%
rd32-v1_68	36	21	24	27	18	5	81.5%
alu-v0_27	36	21	30	29	21	6	79.3%
3_17_13	36	22	21	26	12	7	73.1%
4mod5-v1_24	36	21	36	34	18	7	79.4%
alu-v1_29	37	22	27	25	18	5	80.0%
alu-v1_28	37	22	30	33	24	6	81.8%
alu-v3_35	37	22	33	30	18	6	80.0%

TABLE V: Comparison of MCTS-Depth with $t|ket\rangle$ [7] on IBM Q20 with naive initial mappings.

Circuit Name	Input Gates	Input Depth	Gates Added Pytket	Depth Added Pytket	Gates Added MCTS-Depth	Depth Added MCTS-Depth	Improvement
alu-v2_33	37	22	27	28	21	6	78.6%
alu-v4_37	37	22	30	30	21	6	80.0%
millar_11	50	29	27	32	12	6	81.3%
decod24-v0_38	51	30	36	41	15	5	87.8%
alu-v3_34	52	30	45	48	24	7	85.4%
decod24-v2_43	52	30	36	42	15	4	90.5%
mod5d2_64	53	32	51	53	36	10	81.1%
4gt13_92	66	38	54	63	42	9	85.7%
4gt13-v1_93	68	39	45	50	48	11	78.0%
one-two-three-v2_100	69	40	54	62	30	10	83.9%
4mod5-v1_23	69	41	60	66	66	11	83.3%
4mod5-v0_18	69	40	51	61	48	13	78.7%
one-two-three-v3_101	70	40	57	61	30	13	78.7%
4mod5-bdd_287	70	41	45	51	27	6	88.2%
decod24-bdd_294	73	40	45	48	27	9	81.3%
4gt5_75	83	47	63	63	57	14	77.8%
alu-v0_26	84	49	72	76	42	7	90.8%
rd32_270	84	47	51	53	45	13	75.5%
alu-bdd_288	84	48	39	32	75	10	68.8%
decod24-v1_41	85	50	69	76	30	8	89.5%
4gt5_76	91	56	66	74	54	10	86.5%
4gt13_91	103	61	63	65	39	7	89.2%
4gt13_90	107	65	69	70	45	7	90.0%
alu-v4_36	115	66	72	84	54	17	79.8%
4gt5_77	131	74	54	48	45	14	70.8%
one-two-three-v1_99	132	76	102	107	72	17	84.1%
rd53_138	132	56	54	46	117	29	37.0%
one-two-three-v0_98	146	82	84	99	96	18	81.8%
4gt10-v1_81	148	84	102	109	90	13	88.1%
decod24-v3_45	150	84	123	136	90	15	89.0%
aj-e11_165	151	86	84	89	84	17	80.9%
4mod7-v0_94	162	92	99	112	93	17	84.8%
alu-v2_32	163	92	105	117	63	18	84.6%
4mod7-v1_96	164	94	102	117	72	17	85.5%
cnt3-5_179	175	61	162	91	159	28	69.2%
mod10_176	178	101	87	90	105	20	77.8%
4gt4-v0_80	179	101	96	102	69	10	90.2%
4gt12-v0_88	194	108	114	111	54	14	87.4%
0410184_169	211	104	147	112	132	20	82.1%
4_49_16	217	125	132	150	102	13	91.3%
4gt12-v1_89	228	130	126	116	63	14	87.9%
4gt4-v0_79	231	132	75	63	69	9	85.7%
hwb4_49	233	134	159	174	93	19	89.1%
4gt4-v0_78	235	137	81	68	105	15	77.9%
mod10_171	244	139	162	171	90	16	90.6%
4gt12-v0_87	247	131	90	80	84	23	71.3%
4gt12-v0_86	251	135	93	82	72	20	75.6%
4gt4-v0_72	258	137	165	160	66	15	90.6%
4gt4-v1_74	273	154	198	217	111	24	88.9%
mini-alu_167	288	162	210	235	132	31	86.8%
one-two-three-v0_97	290	163	225	259	111	39	84.9%
rd53_135	296	159	165	165	138	29	82.4%
ham7_104	320	185	63	46	102	26	43.5%

TABLE V: Comparison of MCTS-Depth with $t|ket\rangle$ [7] on IBM Q20 with naive initial mappings.

Circuit Name	Input Gates	Input Depth	Gates Added Pytket	Depth Added Pytket	Gates Added MCTS-Depth	Depth Added MCTS-Depth	Improvement
decod24-enable_126	338	190	177	192	105	27	85.9%
mod8-10_178	342	193	156	162	57	15	90.7%
4gt4-v0_73	395	227	282	312	87	22	92.9%
ex3_229	403	226	234	234	69	20	91.5%
mod8-10_177	440	251	195	188	105	19	89.9%
alu-v2_31	451	255	303	331	141	37	88.8%
C17_204	467	253	210	214	99	24	88.8%
rd53_131	469	261	240	258	75	28	89.1%
alu-v2_30	504	285	273	289	99	43	85.1%
mod5adder_127	555	302	255	263	138	36	86.3%
rd53_133	580	327	348	365	123	34	90.7%
majority_239	612	344	219	229	150	31	86.5%
ex2_227	631	355	345	361	156	28	92.2%
cm82a_208	650	337	330	303	195	59	80.5%
sf_276	778	435	348	365	111	36	90.1%
sf_274	781	436	339	417	51	26	93.8%
con1_216	954	508	501	512	291	66	87.1%
rd53_130	1043	569	456	442	261	65	85.3%
f2_232	1206	668	558	572	285	56	90.2%
rd53_251	1291	712	627	693	303	65	90.6%
hwb5_53	1336	758	510	537	384	97	81.9%
radd_250	3213	1781	1341	1345	882	160	88.1%
rd73_252	5321	2867	1983	1952	1347	318	83.7%
cycle10_2_110	6050	3386	2697	2788	1518	344	87.7%
hwb6_56	6723	3736	2598	2688	1563	390	85.5%
cm85a_209	11414	6374	4083	4032	2529	588	85.4%
rd84_253	13658	7261	5853	5776	3954	963	83.3%
root_255	17159	8835	7137	7209	3957	1135	84.3%
mlp4_245	18852	10328	8607	8295	5535	1210	85.4%
urf2_277	20112	11390	10524	10247	10224	2674	73.9%
sym9_148	21504	12087	8190	8495	1290	133	98.4%
hwb7_59	24379	13437	11523	11718	5178	1227	89.5%
clip_206	33827	17879	13992	13897	8670	2306	83.4%
sym9_193	34881	19235	15213	15159	7473	1742	88.5%
dist_223	38046	19694	15576	15656	8622	2581	83.5%
sao2_257	38577	19563	14928	14852	8691	2739	81.6%
urf5_280	49829	27822	22113	21636	19401	5154	76.2%
urf1_278	54766	30955	24948	24119	20541	5564	76.9%
sym10_262	64283	35572	28071	27923	15855	3369	87.9%
hwb8_113	69380	38717	26043	26039	17043	3462	86.7%
Summary	554497	303469	237471	236312	151530	37794	84.0%

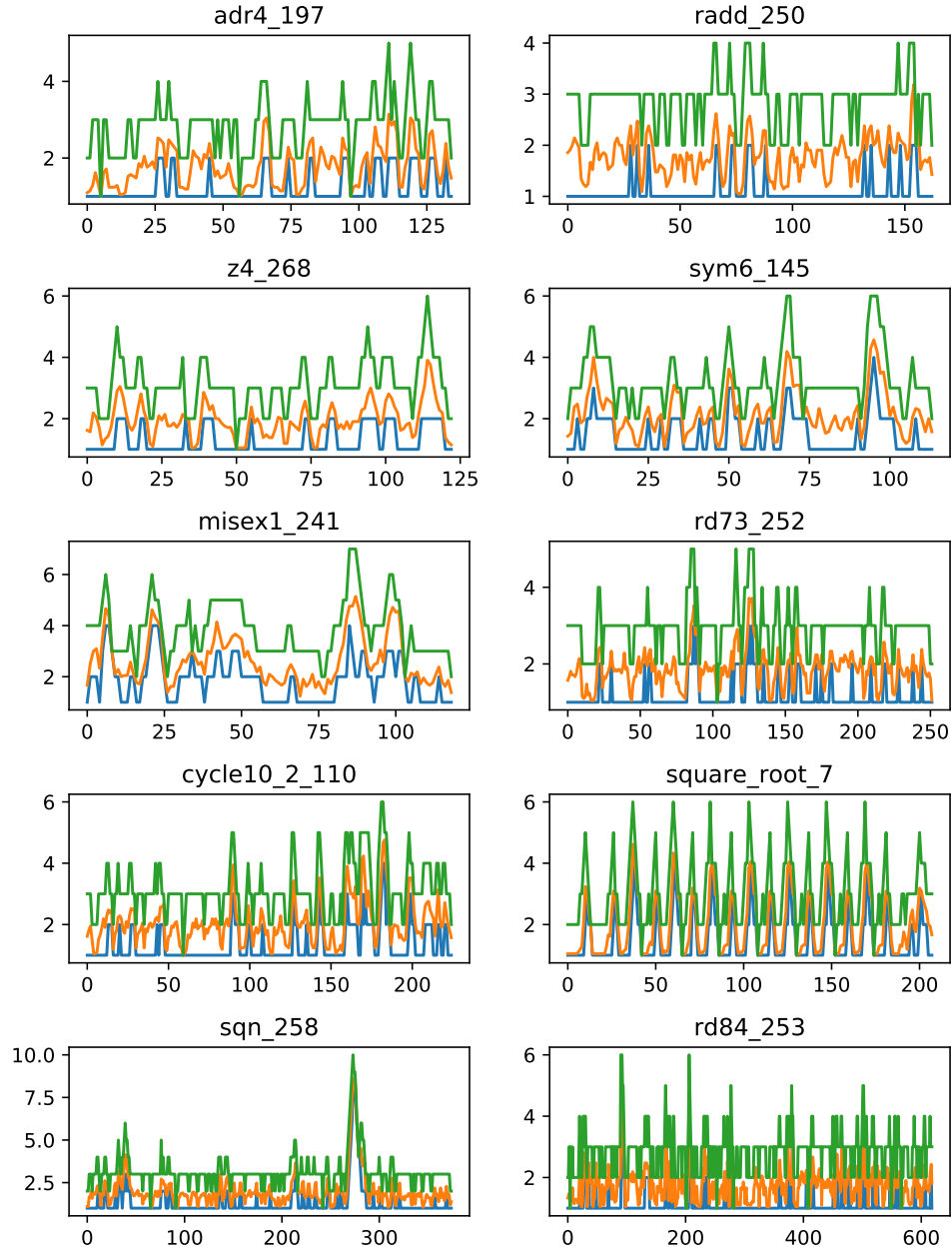


Fig. 13. Results of search depths on small benchmark set with parameters setting as described in paper. The horizontal and vertical axis represent rounds for *Decision* and search depth, respectively. The green, orange and blue line represent, respectively, the maximum, average and minimum depth among all *Selections* before each *Decision*.